Available online at www.sciencedirect.com
SCIENCE DIRECT®
Earth and Planetary Science Letters 245 (2006) 538–550
EPSL
www.elsevier.com/locate/epsl

Experimental observation of magnetosome chain collapse in magnetotactic bacteria: Sedimentological, paleomagnetic, and evolutionary implications

Atsuko Kobayashi [a,*], Joseph L. Kirschvink [b], Cody Z. Nash [b], Robert E. Kopp [b], David A. Sauer [b,1], L. Elizabeth Bertani [c], Wim F. Voorhout [d], Takahisa Taguchi [a]

[a] *Research Institute for Cell Engineering, National Institute of Advanced Industrial Science and Technology, 1-8-31 Midorigaoka, Ikeda, Osaka 563-8577, Japan*
[b] *Division of Geological and Planetary Sciences, California Institute of Technology 170-25, Pasadena, CA 91125, USA*
[c] *Division of Biology, California Institute of Technology 170-25, Pasadena, CA 91125, USA*
[d] *FEI Electron Optics, Applications Laboratory, P.O. Box 80066, 5600KA, Eindhoven, The Netherlands*

Received 6 December 2005; received in revised form 16 March 2006; accepted 23 March 2006
Available online 9 May 2006
Editor: V. Courtillot

Abstract

Magnetotactic bacteria precipitate intracellular crystals of single-domain magnetite (Fe_3O_4) and/or greigite (Fe_3S_4), which have often been implicated in carrying the natural remanent magnetization (NRM) of freshwater and marine sediments. In vivo, the magnetic crystals are usually aligned in chains such that their moments add together, generating net cellular moments high enough to rotate the cells passively to align with the geomagnetic field. A magnetostatic/biophysical analysis demonstrates that this arrangement is out of dynamic equilibrium and would collapse spontaneously without a support mechanism. Past rock magnetic analyses of shallow water marine carbonates suggest that partial collapse does occur during diagenesis and dolomitization.

To calibrate this effect we induced magnetosome chain collapse in *Magnetospirillum magnetotacticum* strain MS-1 by progressive sonification and treatment with detergents and monitored the changes with rock magnetic analysis and TEM. Although it has been speculated that the cell wall and associated membrane structures act to prevent magnetosome chain collapse, our data indicate that magnetosome linearity persists long after cells are disrupted. This is consistent with prior observations that in some magnetotcocci the magnetosome chains pass through the cell interior, precluding continuous contact with the cell wall and implying additional support structures exist in some species.

Using TEM tomographic reconstructions prepared with a magnetic technique that prevents chain collapse, we examined the three dimensional ultrastructure of magnetosomes without the problem of post-mortem magnetosome motion. This method revealed the presence of an intracellular organic sheath beyond that of actin-like filaments reported recently that follows the chain of magnetosomes, which we postulate evolved to hold the crystals in place and enhances their ability to preserve NRM in sediments. As the genomes of two magnetotactic bacteria contain several apparent homologues of known eukaryotic cytoskeletal proteins, natural selection for magnetotaxis may have played a role in the evolution of precursors to the eukaryotic cytoskeleton.

* Corresponding author. Tel.: +81 72 751 9524; fax: +81 6 6844 0595.
E-mail address: kobayashi-a@aist.go.jp (A. Kobayashi).
[1] Present address: Department of Pathology, Oregon Health and Science University, Portland, OR 97202, USA.

doi:10.1016/j.epsl.2006.03.041

The presence of this sheath is also consistent with the observation of electron translucent material associated with putative magnetofossil chains in ALH84001.

Keywords: rock magnetism; paleomagnetism; magnetotactic bacteria; cytoskeleton; evolution

1. Introduction

In living magnetotactic bacteria, individual magnetite crystals are formed within a string of vesicles, each of which is a lipid-bilayer membrane [1–3]. Numerous optical and behavioral observations show that the in vivo magnetite crystals are aligned in linear chains, allowing virtually all of their dipole magnetic moments to sum linearly, bringing the total magnetic moment per cell to values close to that expected from the quantity of single domain magnetite or greigite within them [3–9]. Natural selection for magnetotaxis has presumably optimized the use of iron within many of these cells, as it is a scarce nutrient that, in aerobic environments, requires an energy-expensive active transport system [10]. However, the ability to keep the magnetosomes aligned is a biophysical puzzle because lipid-bilayer membranes are fluidic, and the magnetite crystals ought to be able to move and rotate freely within their vesicles. Similarly, magnetite-containing vesicles should be able to move relative to each other in response to local magnetostatic interactions unless otherwise constrained [11].

One model suggests that the apparent stability of magnetosome chains may be due to a combination of the magnetosome shape and elastic properties of biological membranes [12,13]. This model is based on 2D TEM images of in situ magnetosomes that suggested the crystal shapes were simple right cylinders or rectangular prisms with flat ends. However, subsequent HRTEM studies of magnetosomes have revealed that the ends are, in fact, not square – they are typically 'rounded' by the expression of {100}, {110}, {111} and possibly other crystal faces [14,15]. This geometry acts to minimize the stabilizing effect of the flat ends and implies that magnetosome chains are intrinsically unstable – as the rounded ends of two adjacent crystals start to rotate out of linear alignment, there is no barrier to inhibit chain collapse. Thermal fluctuations in the membrane surface also appear large enough to initiate chain collapse [16]. This rounding at magnetosome ends has been explained as a mechanism for improving the saturation magnetization, and hence the biological efficiency of iron utilization, by eliminating spin-vortex 'flower-structures' that arise near sharp corners of single-domain crystals [17,18].

Although numerous TEM images show rapidly fixed magnetotactic bacteria with apparently linear chains, Vali and Kirschvink [19] note that this is not always the case in many bacteria. Despite the evidence for linear chains in vivo, chains do collapse during typical preparation for TEM; this has been independently predicted and observed by Philipse and Maas [20]. In particular, even apparently linear images of such chains, when viewed via a single 2D electron shadow image in a TEM, cannot detect oscillations in the vertical plane. Linear chains can in principle provide a strong and stable natural remanent magnetization (NRM), whereas highly interacting clumps of SD particles would have both lower intensity and lower stability. The ability to avoid clumping is critically important for understanding how magnetofossil-rich sediments are able to preserve NRM.

Using rock magnetic techniques, McNeill and Kirschvink [21] have documented magnetofossil chain collapse in carbonaceous marine sediments from the Bahamas, where the process reduces the intensity and stability of the NRM. In particular, increasing levels of diagenesis, calcification, and dolomitization inhibited the acquisition of anhysteretic remanent magnetization (ARM), implying that the magnetostatic interaction between magnetic particles was increasing [22]. However, it was not clear from that study how the microscopic arrangements of the magnetofossils were changing, as the procedures for extracting the bacterial magnetite particles (magnetofossils) from sediments result in clumped aggregates of particles.

Without some form of rigid support, linear chains of single-domain magnetite crystals will collapse spontaneously because they are physically unstable. For elongate crystals, magnetostatic energy calculations [10,20] show that the collapse of chains into clumps of crystals is favored strongly, as, by reducing the center-to-center spacing of the dipoles, it can reduce the magnetostatic potential energy of the cell by $\sim 10^4 kT$ (where kT, the product of the Boltzmann constant and the absolute temperature, is the one-dimensional thermal background energy). Paired anti-parallel magnetosome crystals have been seen in TEM images of cells with elongate crystal morphologies (e.g., [19]). Although equant crystals are more stable in a chain configuration than in the paired anti-parallel configuration, for any

crystal shape the overall magnetostatic energy of long chains of particles is minimized when the chains collapse into small loops.

At least two mechanisms could prevent the collapse of these chains. First, proteins or some other organic macromolecules could hold adjacent crystals together like strings by anchoring themselves into the internal structure of each crystal. These anchor strings would have to pass completely through two lipid bilayer membranes, be of the correct length to minimize in-chain wobble, and be strong or numerous enough to overcome forces producing chain collapse. The ends of the chain would then be attached to the structural components of the cell wall, to transmit the rotational magnetic torque to the entire cell body [5]. The other possibility is that the cells might produce a larger organic 'sheath' that would enclose the entire chain of magnetosomes within a rigid superstructure, preventing their collapse [23,24]. If held in a line, individual crystals would be inhibited from rotating within their encapsulating membrane by magnetic interactions with adjacent particles, rather than with embedded strings. This sheath structure could then be anchored to various cytoskeletal filaments that run along the inside of the bacterial cell membranes to provide cell shape and rigidity [25,26], thereby transferring the magnetic torque needed for navigation to the entire cell. A protein in the magnetosome membrane, MamJ, has been shown to be necessary for alignment of magnetosomes along a filamentous structure in the magnetotactic bacteria *Magnetospirillum gryphiswaldense* [27], and in *Magnetospirillum magneticum* filaments of an actin-like protein, MamK, appear to run the length of the cell [28], supporting the idea that external structures constrain the motion of the magnetosomes

To distinguish between these possibilities, we first performed a series of experiments with cultures of *M. magnetotacticum* strain MS-1, which we subjected to increasing cellular disruption using ultrasonic and chemical methods; TEM imaging and rock magnetic experiments were coupled to monitor the progress of chain collapse. Next, we developed a simple method to inhibit the magnetostatic motion of the chains during preparation for TEM, from which we can then derive accurate parameters such as magnetosome volume and spacing using energy-filtered TEM. These data are then used to estimate the energies and forces involved in the stability of magnetosome chains. Next, we report on the tomographic 3D reconstructed imaging of cells prepared in this fashion. Finally, we report results of our search for supporting structures along the magnetosome chains.

2. Materials and methods

2.1. Materials

Cultures of the magnetotactic bacterium *M. magnetotacticum* strain MS-1 were obtained from the American Type Culture Collection (ATCC 31632), and grown according to their recommendations. When cultures had reached their log-growth phase, magnetotactic cells were harvested from aggregations accumulating next to magnets held at the side of the culture flasks using Pasteur pipettes modified to have a bent tip, as done by Moench and Konetzka [29].

2.2. Disaggregation method

About 30 μl aliquots of cell pellets were placed in acid-washed plastic Eppendorf tubes, and diluted in an equal volume of deionized water. Disruption began by inserting the stainless-steel probe of a Fischer Scientific Sonic Dismembrator 550® into the liquid, at increasing levels of exposure/pulse cycles. To further disrupt the cells by disrupting the membranes, we added steps including sodium dodecyl sulfate (SDS). In order of progressive disruption, our samples reported here were treated in the following sequence: (a) wild-type cells with no disruption, (b) disruption with 200 pulses at 8 s each, (c) 400 pulses at 7 s each, (d) 0.05% SDS, and 75 pulses at 5 s each, and (d) 0.05% SDS, and pulsed every 4 s for 10 min. The pellets frozen in the Eppendorf tubes were subjected to a standard series of rock magnetic analyses as noted below.

2.3. Magnetometry measurements

These rock magnetic experiments were done at −20 °C, using a vertically mounted 2G Enterprises® SQUID magnetometer housed in a magnetically shielded clean room at Caltech, which was equipped with a refrigerated sample access chamber. A stepping motor raised and lowered the sample from above on thin monofilament line, moving it between the coils and the SQUID sense region. Experiments involved the following techniques: (1) Alternating-field (AF) demagnetization up to 100 mT was done with a commercial degausser (Applied Physics Systems® of Menlo Park, CA), using a solenoid mounted at the top of the sample path. (2) To supply DC biasing fields between 0 and 2 mT, a custom-built Lee-Whiting-4 coil system [30,31] was mounted over the Af solenoid, but within the μ-metal shielding. (3) Isothermal remanent magnetizations (IRMs) were applied using a capacitive impulse magnetizer (ASC

Scientific®, Model IM-10, with the design of Kirschvink [32]), which discharged through a solenoid mounted along the sample path above the AF coil. All of these devices were run automatically by a dedicated computer that had been programmed to do, in sequence, the following progressive magnetization and demagnetization experiments: (1) ARM acquisition in a 100 mT AF field, with biasing fields up to 2 mT; (2) AF of the maximum ARM up to 100 mT; (3) IRM acquisition up to 100 mT; and (4) AF of the IRM. These data constitute the basic magnetic granulometry techniques of Cisowski [22] and the ARM modification of the Lowrie–Fuller test [33]. Control measurements were done with similar acid-washed Eppendorf tubes filled with sterile growth media to ensure that the magnetic signals were due to the bacteria and not to the contaminants from the culture media or disposable labware [34].

2.4. Transmission electron microscopy

For the disaggregation experiments, we preserved the disrupted configurations for both TEM and rock magnetic experiments by rapidly blotting small drops of the cell suspension onto hydrophilic TEM grids, while at the same time freezing the remaining cell suspension rapidly in liquid nitrogen for rock magnetic analyses. The grids were examined at moderate magnification on a Zeiss-9 TEM to assess chain linearity vs. clumping. For the experiments with aligned chains, the samples were prepared by negative staining or conventional embedding procedures (e.g., [35]) as described elsewhere. We stabilized magnetotactic bacteria with a strong background magnetic field maintained during the entire fixation and TEM sample preparation process to prevent chain collapse with a pair of NdFeB disc magnets, 2 mm in diameter separated by a 3.7 mm gap, which produced a measured minimum magnetic field in the center of ~100 mT (see Fig. 3 for details). The magnetostatic alignment of the chains also facilitates TEM-based ultrastructural analysis, as ultrathin sections can be made from embedded samples with a diamond knife cutting parallel to the chain length.

Samples were prepared by negative staining or conventional embedding procedures (e.g., [35]). All cells collected by magnets were first fixed with 1% glutaraldehyde and 4% paraformaldehyde in 0.1 M phosphate buffer (PB) at pH 7.4 for half an hour. Cells were then post-fixed in 1% osmic acid/0.1 M PB for 1 h and run through the standard epon embedding procedure. Samples were cut into 200 nm thin sections and 70 nm ultrathin sections parallel to the chain length by a Leica Ultracut UCT with a diamond knife. Each specimen was collected on Cu grid supported by carbon films, then post-stained with 2% uranyl acetate/lead citrate. A few cells were negatively stained with tungsten phosphate as noted below.

We used a Tecnai F20G2Twin, equipped with Gatan energy filter GIF2002 and multi-scan CCD camera (1024×1024, 24 μm/pixel), comprising a phosphor fiber-optically coupled, operating at 100 kV. The filter was tuned for the chromatic–geometric aberrations, prior to image acquisitions at the magnification. The images of iron were acquired with an energy filter slit width of 25 eV for mapping the Fe–L edge at 708 eV. We obtained images with acquisition times of 30 s; our instrument sample holder has an rms maximum drift of ~0.5 nm/min. We corrected for baseline change using the standard 3-window correction method that produces an optimum isolation of the Fe-signal from the background. All images were corrected for the CCD's dark current and gain variations and processed by Digital Micrograph 3.3 for size determinations.

2.5. Electron tomographic imaging

In the magnetotactic bacteria, structures supporting the magnetosome chains should be visible with suitable TEM techniques, assuming that the spatial relationship between the crystal chains and the supporting materials can be preserved post-mortem. Automated electron microscopic tomographic imaging [36,37] can then provide another tool for examining the continuity between the magnetosome chains and internal cellular structures, particularly when the structure has a directional irregularity. A series of projection images is acquired by tilting the specimen incrementally to high tilt angles around an axis perpendicular to the electron beam. From this series of images, a 3D tomogram with nanometer-scale resolution can be reconstructed. For our tomographic study, we used a Tecnai Sphera with a sample holder, tilting at 1° increments through ±65°, operating at 200 kV. For a 200 nm spherical sample incrementally tilted up to ±65° with 1° steps, the limiting resolution is around 5 nm [38]. The drift of the holder position was calibrated prior to the data acquisition for experimental samples. Image data were processed using Xplore3D software fort 3D reconstruction and further processes were done with the AMIRA 3.0 software package.

3. Results

3.1. Dispersion of aligned chains

Figs. 1 and 2 show representative TEM and rock magnetic results from the dispersion experiments. As

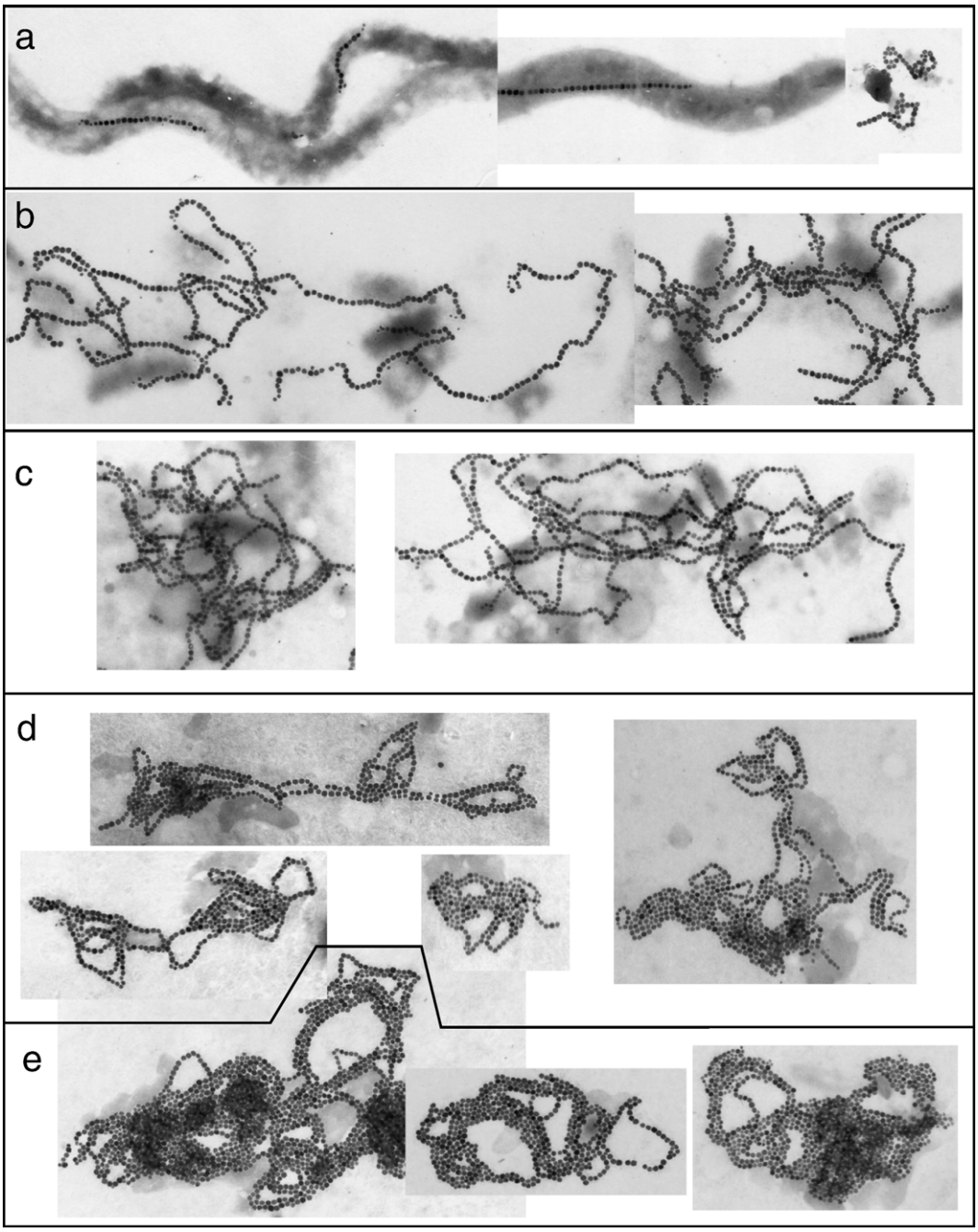

Fig. 1. TEM images of the progressive collapse of the magnetosome chain structures in cells of *M. magnetotacticum* strain MS-1. The order of progressive disruption is arranged vertically such that (a)<(b)<(c)<(d)<(e). Note that both the outer and plasma lipid-bilayer membranes surrounding the cell are lost at the first ultrasonic disruption step used in the (b) preparation; although the magnetosome chains start to bend, they do not collapse. For scale, note that magnetosomes in this strain have a center-to-center separation of approximately 57 nm.

the cells or cell fragments were observed optically to adhere tightly to the hydrophilic surface of the TEM grids before air drying, and the freezing was rapid, it is reasonable to assume that the transfer and freezing procedures had minimal effect on the magnetosome organization, other than compressing 3D loops and clusters onto a 2D TEM grid. Undisrupted cells are shown in Fig. 1a, and the red curves labeled (a) in Fig. 2. The TEM images reveal that progressively increasing levels of ultrasonic disruption and detergent

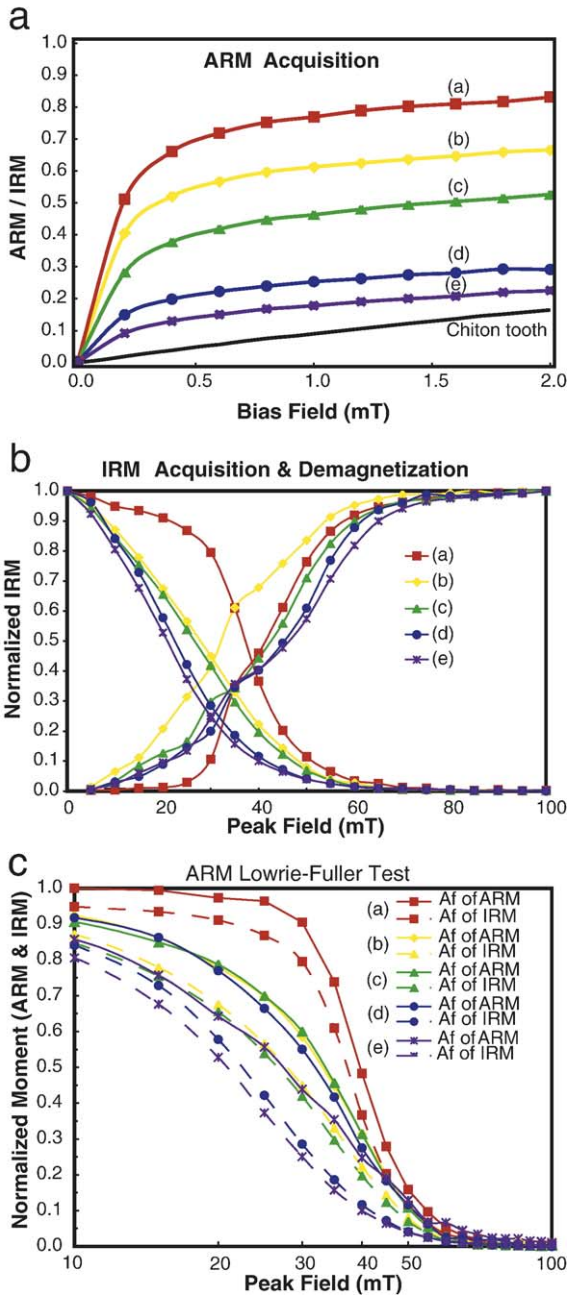

Fig. 2. Rock-magnetic experiments on aliquots of the cells imaged in Fig. 1, with color patterns in rainbow order of increasing disruption. (a) Acquisition of anhysteretic remanent magnetization, (b) Lowrie–Fuller ARM test, (c) comparison of coercivity gain/loss between IRM and ARM.

destruction of the membranes led to an increasing frequency of closed flux-loops and dense clumps. Although the first ultrasonic disruption (b) destroyed most visible cell structures (presumably by popping both the lipid-bilayer membranes which form the cell wall/envelope in Gram-negative bacteria), the chains themselves did not collapse immediately into disordered clumps. Instead, they remain associated with fragments of the cytoplasm until that could be removed by the action of detergents and higher levels of ultrasonic treatment.

Rock magnetic data display a trend of increasing interaction effects that increase with cell disruption, including a lowering of the ARM acquisition rate (Fig. 2a) and a rather abrupt decrease of the median coercivity (Fig. 2b, c). This loss of coercivity is intriguing, because the rather sharp drop-off of the IRM–AF curve between 35 and 45 mT (Fig. 2b and c) happens before the intersection point of the acquisition/demagnetization drops (the interaction "*R*" value of Cisowski [22]). All of the samples pass the Lowrie–Fuller ARM test for single-domain behavior (Fig. 2c): the ARM–AF curves lie above those of the IRM–AF.

3.2. Electron microscopy

As shown in Figs. 3–5, the strong-field embedding technique provides samples with remarkably straight and uniformly parallel magnetosome chains, maximizing the ability to observe cellular material in their vicinity. Close examination of the TEM images prepared in this fashion indicates that the magnetite crystal chains in MS-1 are associated with an electron translucent sheath; this is indicated on the 50–70 nm thick wedge of Fig. 3a and b. Fig. 3c shows results from an electron microscope image of a negatively stained, fixed MS-1 whole cell prepared in this fashion; Fig. 3d is a higher resolution image of one end of this chain. Small red arrows in Fig. 3b and d show the somewhat irregular margins of this apparent sheath material. Detailed measurements indicate that the margins of this sheath are somewhat irregular, but that the sheaths are approximately 100 nm in diameter. This implies that it is not simply an extension of the lipid-bilayer magnetosome membrane that covers each magnetite crystal [1,2], which should only extend ~6 nm from the crystal surfaces, but that it is composed of additional material. Two movies of the tomographic reconstructions are available from the online supplemental information, and stereo pairs of images extracted from these are shown in Fig. 4. An additional tomographic reconstructed image in the Appendix shows the high degree of internal control on the magnetosome spacing and positioning in the bacterial cell.

To estimate the fraction of the cellular volume occupied by the magnetosome chain assembly, we modeled the magnetosomes of Figs. 3 and 5 as regular

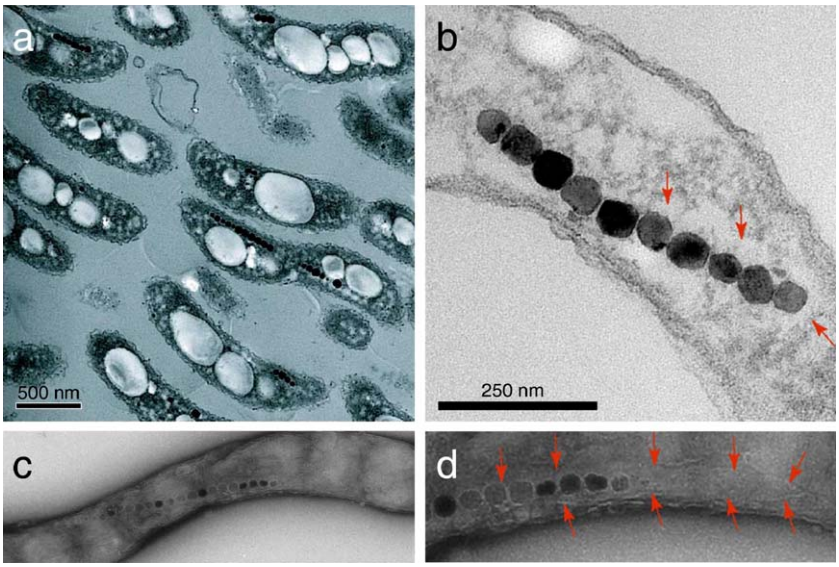

Fig. 3. TEM images of intact cells of MS-1, prepared in the presence of a static, strong magnetic field designed to prevent magnetosome chain collapse. The magnetostatic orientation energy (E_{mo}, in cgs units) of each magnetosome in an external magnetic field, B, is given by their vector dot product, $-\mu \cdot B$, where μ is the particle magnetic moment. (For simplicity in magnetostatic calculations, we prefer to use the Gaussian cgs system and translate our results back into SI units.) If this exceeds the collapse energy (E_c) between two particles separated by a distance x, given by $-\mu^2/x^3$ (see Section 3.3 regarding the biophysics), the chain structure is stabilized; for magnetosomes of *M. magnetotacticum*, strain MS-1, this critical threshold field is ~16 mT. (a and b) ~70 nm thick ultra-thin section of wedge of magnetotactic bacteria embedded in epon, cut parallel to the direction of the applied magnetic field direction. (c) Negatively stained TEM image of an intact bacterial cell, showing the linear chain of electron dense magnetosomes. (d) Enlarged view of the right-hand margin of the magnetosome chain in (c). Red arrow tips in (b) and (d) show the margin of the organic 'sheath' that envelopes the magnetosome chain structures. Only the cells in (c) and (d) were negatively stained with tungsten-phosphate (Nano-W, Nanoprobes).

truncated octahedra ('cubo-octahedra' using the terminology of [39]), and the sheath as a simple cylinder surrounding the magnetosome chain. In the magnetospirilla, numerous studies have shown that the crystals tend to be aligned with their crystal axes parallel to the [111] cubic direction (i.e., they have parallel sets of {111} crystal faces perpendicular to the chain axis). This is not surprising because the [111] axis is the magnetically 'easy' direction, and crystallites growing in the strong local field at the end of a magnetosome chain will spontaneously align in this orientation [11]. As the plane of our TEM sections shown in Figs. 3 and 5 were cut parallel to the direction of the strong field applied by the rare-earth magnets, the crystal dimension measured along the chain axis provides an estimate of the spacing between parallel {111} planes. Since the energy loss at the Fe–L edge at 708 eV is very sharp and our samples have a large signal/noise ratio, we measured the crystal size and spacing by locating the full width half-maximum (FWHM) intensity point in the Fe spectra as shown on the line profile in our Fig. 5.

Measurements of 15 mature crystals from two magnetosome chains like those shown in Fig. 4 yield a mean plane separation of 43.1±4.5 nm, with a center-to-center spacing of 56.8±3.7 nm (1σ errors); the average interparticle gap of ~13.7±2.1 nm is consistent with two unit membranes. This size distribution is in good agreement with the measurements of Devouard et al. [39], who also did not use negative staining but had no 3D control of the chain warping. Our measured interparticle spacing, however, is significantly larger than the 10.0 nm (2×5.0 nm) spacing reported by Gorby et al. [1], which may be a result of the negative staining procedure enhancing the apparent size of the crystals. (Although small, this is an important difference because the magnetostatic forces vary as the inverse fourth power of particle separation.)

To convert from this on-axis {111} planar separation to an estimate of the cubo-octahedral crystal volume involves using geometry; the length of any of the twelve edges of a regular octahedron is √6 times that of the distance from the center to the midpoint of any of the faces. Using a right triangle, the 43 nm average planar spacing corresponds to a regular octahedron with a full vertex-to-vertex edge length of 53 nm. Although the *M. magnetotacticum* crystals are somewhat variable, the six octahedral vertices are

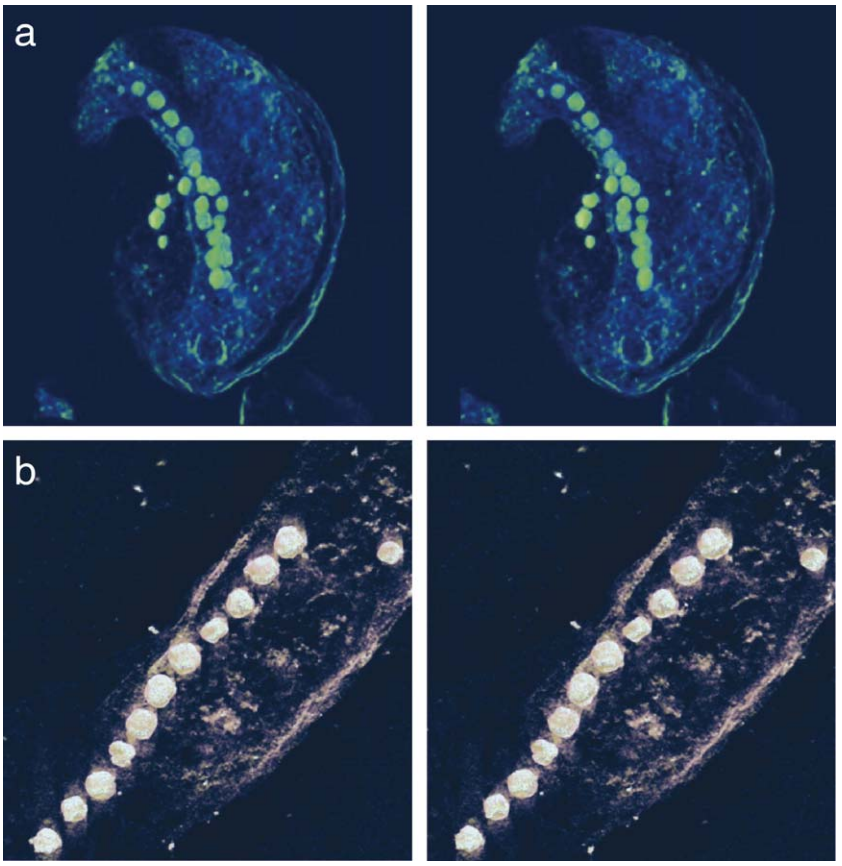

Fig. 4. Stereo frames extracted from tomographic reconstructions of two samples of *M. magnetotacticum* strain MS-1, using 11° tilt between frames. Samples for (a) and (b) are cells from fresh cultures grown with the same techniques, but embedded in the absence and presence, respectively, of a strong magnetic field for keeping the magnetosome chains from collapsing, as mentioned in the text. The specimens were prepared by 200 nm thick sectioning. These correspond to the supplementary data in the Appendix and are available at http://www.gps.caltech.edu/~nascz/Movie_A.mov and http://www.gps.caltech.edu/~nascz/Movie_B.mov.

truncated by {100} and equivalent planes, removing about a third of each edge length at each vertex. This truncation reduces the volume of a perfect octahedron by that of 6 square-based prisms located at each vertex, giving a best volume estimate per crystal of about 62,500 nm^3. For comparison, the diameter of a sphere with an equal volume is about 49 nm. The volume of each magnetosome (magnetite plus membrane) is found in a similar fashion to be about 142,500 nm^3, a bit more than double that of the magnetite alone. Using ~100 nm diameter for the observed sheath, with the length of ~2000 nm seen in Fig. 3a, implies that the entire magnetosome and sheath assembly has a cylindrical volume of ~15.7 million nm^3, which is about 3% of total volume of the cell. This is a significantly larger estimate for the cellular volume devoted to magnetotaxis than previous estimates of about 0.5%, which only considered the magnetosomes [6].

3.3. Biophysics

In vector notation the magnetostatic energy for a pair of interacting magnetic dipoles, $\boldsymbol{\mu}_1$ and $\boldsymbol{\mu}_2$, separated center-to-center by a displacement vector, $\boldsymbol{x}$, is given by:

$$E_{1,2} = \frac{\vec{\boldsymbol{\mu}}_1 \cdot \vec{\boldsymbol{\mu}}_2 - 3(\vec{\boldsymbol{\mu}}_1 \cdot \vec{\boldsymbol{n}})(\vec{\boldsymbol{\mu}}_2 \cdot \vec{\boldsymbol{n}})}{|\boldsymbol{x}|^3} \quad (1)$$

where $\boldsymbol{n}$ is a dimensionless unit direction vector parallel to $\boldsymbol{x}$ [40]. For a pair of equal magnetic dipoles aligned head-to-tail in parallel, the magnetostatic interaction energy (E_{parallel}) reduces to $E=-2\boldsymbol{\mu}^2/\boldsymbol{x}^3$. Similarly, the force ($F$) between the particles is the spatial gradient of the energy, $F=6\boldsymbol{\mu}^2/\boldsymbol{x}^4$. These values are halved for particles that are clumped with their moments in a side-to-side antiparallel configuration; when $\boldsymbol{\mu}_1$ and $\boldsymbol{\mu}_2$ are antiparallel, and both are perpendicular to $\boldsymbol{n}$, $E=-\boldsymbol{\mu}^2/\boldsymbol{x}^3$ and $F=3\boldsymbol{\mu}^2/\boldsymbol{x}^4$. Hence, for two interacting uniformly

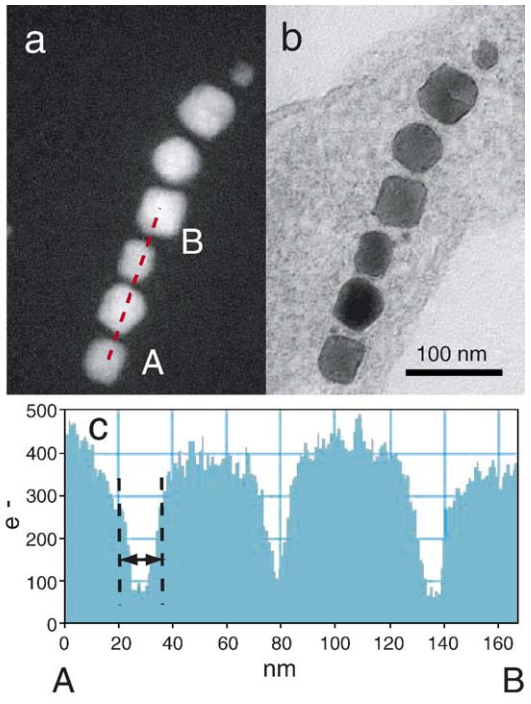

Fig. 5. Image of intact cells of MS-1 for size measurement. (a) Energy-filtered image of iron. (b). Zero loss image of (a). (c) Intensity profile of (a), taken between points A and B in (a). The crystal size is determined by the distance between two edge points at full width half-maximum (FWHM).

magnetized spheres the minimum energy configuration is a head-to-tail configuration. However, for elongate chains of spheres in a negligible background field (e.g., [41]), the magnetostatic energy stored in the field itself becomes large, and this can be reduced by curling the chains into arcs or loops, as clearly happened in the bacterium shown in Fig. 4a.

As noted above, magnetite crystals produced by *Magnetospirillum* strain MS-1 are equivalent to spheres of ~57 nm diameter, and have about 13.7 nm of organic material holding them apart. High-purity, low-defect magnetite such as that precipitated by the magnetotactic bacteria has a saturation magnetization of 4.8×10^5 A/m (480 emu/cm^3, [42]). This yields magnetic moments of the particles of $\sim4.3\times10^{-17}$ A/m^2, and an interparticle compressional force at this separation of about 120 pN. The head-to-tail binding energy is about −550 kT, implying that the arrangement is quite stable against thermal disruption.

4. Discussion

In biomagnetic and rock magnetic studies, the in situ packing geometry of single domain grains is an important, but commonly difficult, parameter to determine. The calibrations shown in Figs. 1 and 2 provide a qualitative guide to how these interaction effects vary as a function of the packing geometry, and provide a start at how to interpret data from natural samples like Recent muds from the Bahamas [21,43]. Of particular interest is the immediate broadening of the coercivity spectra with the initiation of chain curling (the (a) to (b) steps of Figs. 1 and 2). This is accompanied by an abrupt decrease in median coercive field from about 40 to 30 mT, but without a significant drop in the *R* value (the intersection point of the IRM and AF of IRM curves in Fig. 2b, a measure of interparticle interaction [22]). The drop in coercivity is presumably due to the disruption of the linear chain structure – bends in the chains will reduce the stabilizing influence of adjacent magnetic moments to each particle, making it easier for their moments to flip. Upon further disaggregation (the (b) to (c) steps of Figs. 1 and 2), the TEM images indicate that the magnetosomes start to form more regions where the chains line up next to each other in parallel strings; this is accompanied by a slight increase in median coercivity (from about 30 to 35 mT), but with a decrease in the *R* value from 0.42 to 0.32 in Fig. 2b. We suspect that this slight increase in coercivity may be due to the effect of single-domain grains in pairs of adjacent chains stabilizing each other against the external magnetic field (AF or pulse) that is attempting to change their magnetic direction. The drop in *R* value is an indication of the increase in interparticle interaction [22]. Further disruptions including treatment with SDS (the (d) and (e) steps of Figs. 1 and 2) start to destroy the chains, and result in dense 3D clusters of strongly interacting particles. These yield rock magnetic results that progressively resemble the end member of the chiton tooth (*Cryptochiton stelleri*) standard [22,44].

We were surprised at the difficulty of disrupting magnetosome chains in lab cultures. Our initial hope was to disrupt them so completely with the powerful ultrasonic treatment that individual magnetite crystals would separate from each other and become magnetically isolated in the medium, which would allow us to distinguish the magnetic properties of the individual crystals from the properties that arise due to the chain organization. Were this to happen, we would expect that the ARM acquisition curve shown in Fig. 2a would steepen. Instead, progressive disruption from the chain structures dramatically increased the interaction effects, eventually producing the clumped aggregates and loops shown in Fig. 1e.

Comparing these data with the rock-magnetic study of Recent sediments of the Bahama banks [21] indicates that the majority of the Bahama samples have not reached total chain collapse. In this configuration, the particle clumps will still have a net magnetic moment that can align in the geomagnetic field, and, as the sediments are lithified by the precipitation of carbonate cements, this will preserve a stable but weaker NRM, as is often observed in shallow-water carbonates [43]. We also note that post-depositional growth of organisms like *Geobacter* that precipitate extracellular magnetite (e.g., [45]) might also produce this change in the ARM properties of sediments with depth; however, this would lead to an increase in the IRM intensity which is not observed [21].

An important observation here is the fact that the initial disruption of the periplasmic and cytoplasmic membranes did not lead to total collapse of the magnetosome chains. At present, we do not know how these are held together within the cell, although it is often suggested that chain stabilization in the magnetotactic bacteria is produced by continuous physical links between the chain structure and the hydrostatically supported cell walls [1,3,6,46]; this has apparently been observed recently in *M. magneticum* strain AMB-1 [28]. However, if these connections to the membrane were the only method of support, the chains should collapse immediately once the membranes are disrupted. The fact that this collapse requires much more severe treatment, including chemical denaturation agents, demands the presence of additional cytoplasmic and ultrastructural supporting structures that are resistant to disaggregation.

Recent work has demonstrated the presence of filamentous structures along which magnetosomes are aligned in the closely related species *M. gryphiswaldense* MSR-1 [27] and *M. magneticum* AMB-1 [28]. Using cryo-electron tomography, both groups observed filaments that spanned the length of the cell, identified as most likely as the actin homolog, mamK [28], and apparently held in place by the protein product of gene mamJ [27]. In wild-type cells the magnetosomes were aligned along this filament, while in MamJ-deficient mutants the magnetosomes were not associated with the filament, instead forming clumps. With their technique, no sheath structure was observed even in the wild-type. While AMB-1, MSR-1, and MS-1 are closely related, they do have different populations of magnetosome membrane proteins [47], such that they may have different support structures for their magnetosome chains. An intriguing possibility, however, is that MamJ is required for sheath formation, or is one of many components of the sheath itself.

Further evidence for the existence of such supporting structures comes from past freeze-fracture replica studies of magnetic cocci which reveal the presence of linear magnetosome chains that are structurally distant from the cell wall [19]. As shown in Fig. 6a (Fig. 3c of Vali and Kirschvink [19]), these cocci contain large, spherical intracellular storage granules up to 1 μm in size. The freeze-fracture plane in Fig. 6a not only transected the entire cell, exposing a chain of magnetosomes, it also cut through one of these storage granules near its maximum diameter. Hence, the freeze-fracture plane went through the center of the cell, not simply tangential to the edge. As shown schematically in Fig. 6b, the storage sphere contacts the cell membrane on one side, and the magnetosome chain on its other side. In a spherical cell the center does not come near the

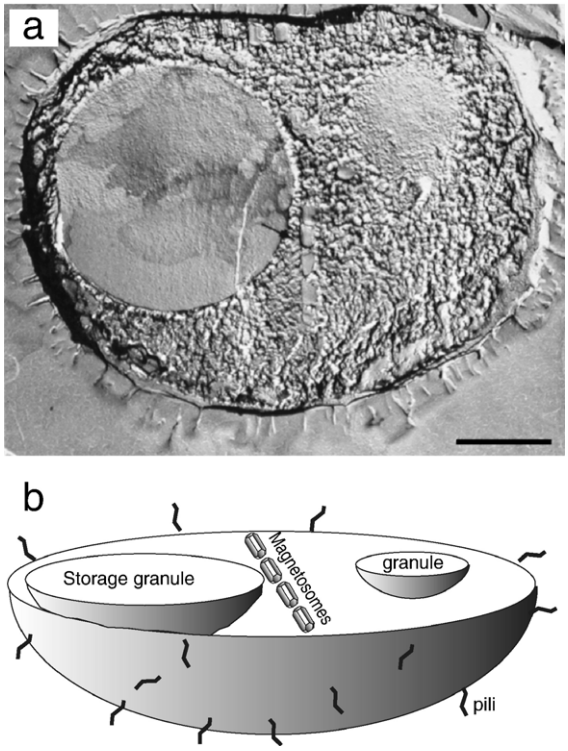

Fig. 6. (a) Magnetic coccus from a freshwater pond near the town of Landshut in Germany (from Vali and Kirschvink [19], reproduced with permission). This is a freeze-etched replica from a transverse section through the center of one of these cells; the large spherical structure is a phosphate granule that has been transacted near its full dimension, indicating that the fracture plane penetrated near the center of the nearly spherical cell. The small arrow indicates the location of the magnetosome chains, which is located in the interior of the cell away from the wall and therefore lacking support. The scale bar is 0.5 μm in length. (b) Schematic diagram of the freeze-fracture image of (a), showing the location of the intracellular storage granules and the magnetosome chain. The central portion of the chain is not adjacent to the cell membrane, but goes through the center of the cell.

bubble-like membrane, so the magnetosome chain shown in Fig. 6a cannot be in contact with it, except possibly at the ends. Since the central portion of the magnetosome chain is not adjacent to the cell membrane, it must have some other means of support, and a significant fraction of the magnetosomes in these magnetococci cannot be attached to the periplasmic membrane as they apparently are in AMB-1 [28]. In addition to our tomographic preparations of Figs. 3 and 5, there are hints of this sheath material present – but not commented upon – in several past publications containing TEM images of various magnetotactic bacteria. In particular, Schübbe et al. [48] report a spontaneous mutant of *M. gryphiswaldense* (MRS-1B) that lost an ~80 kb segment of the magnetosome island and produced no magnetosome vesicles or magnetite crystals. However, as seen on their Fig. 1a, these mutant cells still retain a clear ghost of organic material running along the length of the cells, where the magnetosome chains should have been.

Comparison of the known genetics between the magnetic cocci and magnetospirilla suggests that they probably use similar structures to prevent magnetosome chain collapse. Although uncultured, virtually all magnetic cocci that have been reported so far are members of the alpha-proteobacterial sub-phylum, which also contain the magnetospirilla. The nearly complete genome of the magnetic cocci MC-1 contains virtually all of the genes in the magnetosome island found in the magnetospirilla, indicating that they share large elements of their magnetosome formation pathways. However, the genomes of the closely related magnetospirilla strains AMB-1 and MS-1 differ in size by nearly 300 kb [49,50], The apparent association of the magnetosome chain structures with the cytoplasmic membrane in the magnetospirilla most likely results from the cell shape. A 2 μm long rod, placed inside a right circular cylinder of about the same length that is then twisted a turn or two (producing the typical structure of a spirillum), will appear to be tangent to the cell wall. Hence a genetic defect that inhibits or minimizes separation of new magnetosome vesicles budding off from the membrane might not be selected against strongly in the magnetospirilla, but would greatly damage the magnetococci. As noted by Vali and Kirschvink [19], endocytosis of this sort was thought to be an exclusively eukaryotic trait.

Although the structure remains uncharacterized, our TEM study of uncollapsed cells reveals the presence of an intracellular magnetosome sheath structure that occupies a significant fraction of the cellular volume. Our failure to image eukaryotic-style internal cytoskeletal fibers using fixing and staining techniques capable of detecting them in eukaryotes [26] implies that either these proteins are only rarely expressed in strain MS-1 or are not generally assembled in the same fashion as they are in the closely related strains GSR-1 and AMB-1 or in their eukaryotic cousins. As noted earlier, the MS-1 genome is missing ~300 kb compared to AMB-1, and although the mamJ and mamK genes are present, their expression could be quite different. In this light it is interesting to note that our tomographic results of stained, epon-embedded cells complement and extend the recent studies of Scheffel et al. and Komeili et al. [27,28], who both used cryoTEM on unstained cells of *M. gryphiswaldense* (with incomplete information from the missing-wedge effect due to the limited tilt-range of ±60°) and *M. magneticum*. Although the classic staining and embedding techniques risk loss of resolution at the sub 5-nm scale, organic structures have such extraordinarily low contrast under any sort of TEM examination that heavy-metal staining is needed to enhance them. It is for this reason that the much larger scale structure of the sheath is apparent in our images.

The recently sequenced genome of *M. magnetotacticum* contains 4 *ftsZ* homologues of tubulin and two *mreB* homologues of actin. Of these genes encoding potential structural proteins, one *mreB* gene is highly conserved among the genomes of magnetic coccus MC-1, *M. magnetotacticum*, and *M. gryphiswaldense*. The highly conserved actin homologue is also part of a larger group (the *magnetosome island*) of conserved genes containing 18 proteins known to be located on the magnetosome [47,51]. The conserved MreB-like protein, named MamK in *M. gryphiswaldense*, is not bound to the magnetosome membrane in extracted magnetosomes [47]. The sequence similarity of MamK to MreB and its disconnection from the magnetosome have led to the speculation that it may be involved in the structural control of the magnetosome chain [48]. On the other hand, it is possible that MamK is not involved in the sheath structure and that the sheath is composed of something entirely different, such as a glycoprotein matrix. Future biochemical and genetic work will be able to determine the composition of the sheath.

The nearly identical appearance of magnetosome chains in bacteria to those widespread in eukaryotic cells ranging from protists [52,53] to the magnetoreceptor cells of animals [54–57] has led to the hypothesis that the mechanisms for producing magnetosomes share a common ancestry [58]. Hence the jump from cytoskeletal filaments arranged along the internal cell wall of bacteria to the role of positioning and

organizing intracellular vacuoles may have been driven by natural selection for magnetotaxis as well as endosymbiotic events in the evolution of the eukaryotic cell. Although there may be no direct homology between the proteins in the magnetosome sheath and the eukaryotic cytoskeleton, the magnetosome structures could provide a stabilizing framework for the evolution of these other scaffolding materials.

The presence of this sheath is also compatible with the observation of Friedmann et al. [13] that the chains of magnetite crystals observed in the magnetite-rich rims of carbonate blebs in the Martian meteorite ALH84001 are, on occasion, encapsulated by an electron-transparent layer of presumed organic composition. If their interpretation of these structures as magnetofossil chains is correct, this transparent material could be the degradation product of the sheath reported here.

Acknowledgments

This work was partially supported by funds from a NEDO (New Energy and Industrial Technology Development Organization, Japan) Fellowship to A.K., grants NIH 1-RO1-ES-06652, and EPRI-RP2965 to JLK. We thank H. Vali of McGill University for permission to use Fig. 6a.

Appendix A. Supplementary data

Supplementary data associated with this article can be found, in the online version, at doi:10.1016/j.epsl.2006.03.041.

References

[1] Y.A. Gorby, T.J. Beveridge, R.P. Blakemore, Characterization of the bacterial magnetosome membrane, J. Bacteriol. 170 (1988) 834–841.
[2] N. Nakamura, K. Hashimoto, T. Matsunaga, Immunoassay method for the determination of immunoglobulin-G using bacterial magnetic particles, Anal. Chem. 63 (1991) 268–272.
[3] D.A. Bazylinski, R.B. Frankel, Magnetosome formation in prokaryotes, Nat. Rev., Microbiol. 2 (2004) 217–230.
[4] A.J. Kalmijn, R.P. Blakemore, The magnetic behavior of mud bacteria, in: K. Schmidt-Koenig, W.T. Keeton (Eds.), Animal Migration, Navigation and Homing, Springer Verlag, New York, 1978, pp. 354–355.
[5] R.B. Frankel, R.P. Blakemore, Navigational compass in magnetic bacteria, J. Magn. Magn. Mater. 15 (1980) 1562–1564.
[6] R.P. Blakemore, Magnetotactic bacteria, Annu. Rev. Microbiol. 36 (1982) 217–238.
[7] M. Hanzlik, M. Winklhofer, N. Petersen, Spatial arrangement of chains of magnetosomes in magnetotactic bacteria, Earth Planet. Sci. Lett. 145 (1996) 125–134.
[8] R.E. Dunin-Borkowski, M.R. McCartney, R.B. Frankel, D.A. Bazylinski, M. Posfai, P.R. Buseck, Magnetic microstructure of magnetotactic bacteria by electron holography, Science 282 (1998) 1868–1870.
[9] M. Hanzlik, M. Winklhofer, N. Petersen, Pulsed-field-remanence measurements on individual magnetotactic bacteria, J. Magn. Magn. Mater. 248 (2002) 258–267.
[10] J.L. Kirschvink, Paleomagnetic evidence for fossil biogenic magnetite in western crete, Earth Planet. Sci. Lett. 59 (1982) 388–392.
[11] J.L. Kirschvink, On the magnetostatic control of crystal orientation and iron accumulation in magnetosomes, Automedica 14 (1992) 257–269.
[12] V.P. Shcherbakov, M. Winklhofer, M. Hanzlik, N. Petersen, Elastic stability of chains of magnetosomes in magnetotactic bacteria, Eur. Biophys. J. Biophys. Lett. 26 (1997) 319–326.
[13] E.I. Friedmann, J. Wierzchos, C. Ascaso, M. Winklhofer, Chains of magnetite crystals in the meteorite ALH84001: evidence of biological origin, Proc. Natl. Acad. Sci. U. S. A. 98 (2001) 2176–2181.
[14] P.R. Buseck, R.E. Dunin-Borkowski, B. Devouard, R.B. Frankel, M.R. McCartney, P.A. Midgley, M. Posfai, M. Weyland, Magnetite morphology and life on Mars, Proc. Natl. Acad. Sci. U. S. A. 98 (2001) 13490–13495.
[15] S.J. Clemett, K.L. Thomas-Keprta, J. Shimmin, M. Morphew, J.R. McIntosh, D.A. Bazylinski, J.L. Kirschvink, S.J. Wentworth, D.S. McKay, H. Vali, E.K. Gibson, C.S. Romanek, Crystal morphology of MV-1 magnetite, Am. Mineral. 87 (2002) 1727–1730.
[16] F.L.H. Brown, Regulation of protein mobility via thermal membrane undulations, Biophys. J. 84 (2003) 842–853.
[17] J.L. Kirschvink, A seventh criterion for the identification of bacterial magnetofossils, EOS, Trans.-Am. Geophys. Union 82 (2001) s131.
[18] A. Witt, K. Fabian, U. Bleil, Three-dimensional micromagnetic calculations for naturally shaped magnetite: octahedra and magnetosomes, Earth Planet. Sci. Lett. 233 (2005) 311–324.
[19] H. Vali, J.L. Kirschvink, Observations of magnetosome organization, surface structure, and iron biomineralization of undescribed magnetic bacteria: evolutionary speculations, in: R. Blakemore (Ed.), Iron Biominerals, Plenum Press, New York, 1991, pp. 97–116.
[20] A.P. Philipse, D. Maas, Magnetic colloids from magnetotactic bacteria: chain formation and colloidal stability, Langmuir 18 (2002) 9977–9984.
[21] D.F. McNeill, J.L. Kirschvink, Early dolomitization of platform carbonates and the preservation of magnetic polarity, J. Geophys. Res., [Solid Earth] 98 (1993) 7977–7986.
[22] S. Cisowski, Interacting vs. non-interacting single-domain behavior in natural and synthetic samples, Phys. Earth Planet. Inter. 26 (1981) 56–62.
[23] A. Kobayashi, T. Taguchi, Biological control of magnetite crystal formation in the magnetotactic bacteria: hints concerning the possible evidence from ALH84001 for life on Mars, Geochim. Cosmochim. Acta 66 (2002) A408.
[24] A. Kobayashi, T. Taguchi, Ultrastructure of the magnetite crystal chains in *Magnetospirillum magnetotacticum* (MS-1): evidence from TEM tomography for cytoskeletal supporting structures, Geochim. Cosmochim. Acta 67 (2003) A222.
[25] J. Kurner, A.S. Frangakis, W. Baumeister, Cryo-electron tomography reveals the cytoskeletal structure of *Spiroplasma melliferum*, Science 307 (2005) 436–438.

[26] O. Medalia, I. Weber, A.S. Frangakis, D. Nicastro, G. Gerisch, W. Baumeister, Macromolecular architecture in eukaryotic cells visualized by cryoelectron tomography, Science 298 (2002) 1209–1213.
[27] A. Scheffel, M. Gruska, D. Faivre, A. Linaroudis, J.M. Plitzko, D. Schuler, An acidic protein aligns magnetosomes along a filamentous structure in magnetotactic bacteria, Nature 440 (2006) 110–114.
[28] A. Komeili, Z. Li, D.K. Newman, G.J. Jensen, Magnetosomes are cell membrane invaginations organized by the actin-like protein MamK, Science 311 (2006) 242–245.
[29] T.T. Moench, W.A. Konetzka, A novel method for the isolation and study of a magnetotactic bacterium, Arch. Microbiol. 119 (1978) 203–212.
[30] G.E. Lee-Whiting, Uniform magnetic fields, in: L. Atomic Energy of Canada, (Ed) report CRT-673, Chalk River Project Research and Development, 1957, p. 8p.
[31] J.L. Kirschvink, Uniform magnetic fields and double-wrapped coil systems: improved techniques for the design of biomagnetic experiments, Bioelectromagnetics 13 (1992) 401–411.
[32] J.L. Kirschvink, Ch. 14. Biogenic ferrimagnetism: a new biomagnetism, in: S. Williamson (Ed.), Biomagnetism: An Interdisciplinary Approach, Plenum Press, New York, NY, 1983, pp. 501–532.
[33] H.P. Johnson, W. Lowrie, D.V. Kent, Stability of ARM in fine and course grained magnetite and maghemite particles, Geophys. J. R. Astron. Soc. 41 (1975) 1–10.
[34] A.K. Kobayashi, J.L. Kirschvink, M.H. Nesson, Ferromagnets and EMFs, Nature 374 (1995) 123.
[35] A. Komeili, H. Vali, T.J. Beveridge, D.K. Newman, Magnetosome vesicles are present before magnetite formation, and MamA is required for their activation, Proc. Natl. Acad. Sci. U. S. A. 101 (2004) 3839–3844.
[36] K. Dierksen, D. Typke, R. Hegerl, A.J. Koster, W. Baumeister, Towards automatic electron tomography, Ultramicroscopy 40 (1992) 71–87.
[37] J. Frank, T. Wagenknecht, B.F. McEwen, M. Marko, C.E. Hsieh, C.A. Mannella, Three-dimensional imaging of biological complexity, J. Struct. Biol. 138 (2002) 85–91.
[38] J. Frank, Three Dimensional Electron Microscopy of Macromolecular Assemblies, Oxford University Press, Oxford, 2005, 400 pp.
[39] B. Devouard, M. Posfai, X. Hua, D.A. Bazylinski, R.B. Frankel, P.R. Buseck, Magnetite from magnetotactic bacteria: size distributions and twinning, Am. Mineral. 83 (1998) 1387–1398.
[40] C. Kittel, Introduction to Solid State Physics, John Wiley & Sons, Inc., New York, 1976, 608 pp.
[41] J.S. Yang, C.R. Chang, Magnetic relaxation in chain-of-spheres ferromagnetic particles, J. Magn. Magn. Mater. 239 (2002) 73–75.
[42] D.J. Dunlop, O. Ozdemir, Rock Magnetism: Fundamentals and Frontiers, Cambridge University Press, New York, 1997, 573 pp.
[43] M. Schwartz, S.P. Lund, D.E. Hammond, R. Schwartz, K. Wong, Early sediment diagenesis on the Blake/Bahama Outer Ridge, North Atlantic Ocean, and its effects on sediment magnetism, J. Geophys. Res., [Solid Earth] 102 (1997) 7903–7914.
[44] J.L. Kirschvink, H.A. Lowenstam, Mineralization and magnetization of chiton teeth: paleomagnetic, sedimentologic, and biologic implications of organic magnetite, Earth Planet. Sci. Lett. 44 (1979) 193–204.
[45] H. Vali, B. Weiss, Y.L. Li, S.K. Sears, S.S. Kim, J.L. Kirschvink, L. Zhang, Formation of tabular single-domain magnetite induced by *Geobacter metallireducens* GS-15, Proc. Natl. Acad. Sci. U. S. A. 101 (2004) 16121–16126.
[46] D.L. Balkwill, D. Maratea, R.P. Blakemore, Ultrastructure of a magnetotactic spirillum, J. Bacteriol. 141 (1980) 1399–1408.
[47] K. Grünberg, E.C. Muller, A. Otto, R. Reszka, D. Linder, M. Kube, R. Reinhardt, D. Schüler, Biochemical and proteomic analysis of the magnetosome membrane in *Magnetospitillum gryphiswaldense*, Appl. Environ. Microbiol. 70 (2004) 1040–1050.
[48] S. Schübbe, M. Kube, A. Scheffel, C. Wawer, U. Heyen, A. Meyerdierks, H. Madkour, F. Mayer, R. Reinhardt, D. Schüler, Characterization of a spontaneous nonmagnetic mutant of *Magnetospirillum gryphiswaldense* reveals a large deletion comprising a putative magnetosome island, J. Bacteriol. (2003) 5779–5790.
[49] T. Matsunaga, Y. Okamura, Y. Fukuda, A.T. Wahyudi, Y. Murase, H. Takeyama, Complete genome sequence of the facultative anaerobic magnetotactic bacterium *Magnetospirillum* sp. strain AMB-1, DNA Res. 12 (2005) 157–166.
[50] L.E. Bertani, J. Weko, K.V. Phillips, R.F. Gray, J.L. Kirschvink, Physical and genetic characterization of the genome of *Magnetospirillum magnetotacticum*, strain MS-1, Gene 264 (2001) 257–263.
[51] K. Grünberg, C. Wawer, B.M. Tebo, D. Schüler, A large gene cluster encoding several magnetosome proteins is conserved in different species of magnetotactic bacteria, Appl. Environ. Microbiol. 67 (2001) 4573–4582.
[52] D.A. Bazylinski, D.R. Schlezinger, B.H. Howes, R.B. Frankel, S.S. Epstein, Occurrence and distribution of diverse populations of magnetic protists in a chemically stratified coastal salt pond, Chem. Geol. 169 (2000) 319–328.
[53] R.B. Frankel, F.F.T. Dearaujo, M.A. Pires, C.E.M. Bicudo, Magnetotaxis and magnetite in algae, Biophys. J. 49 (1986) A75.
[54] S. Mann, N.H.C. Sparks, M.M. Walker, J.L. Kirschvink, Ultrastructure, morphology and organization of biogenic magnetite from sockeye salmon, *Oncorhynchus nerka* – implications for magnetoreception, J. Exp. Biol. 140 (1988) 35–49.
[55] C.E. Diebel, R. Proksch, C.R. Green, P. Nielson, M.M. Walker, Magnetite defines a magnetoreceptor, Nature 406 (2000) 299–302.
[56] J.L. Kirschvink, M.M. Walker, C.E. Diebel, Magnetite-based magnetoreception, Curr. Opin. Neurobiol. 11 (2001) 462–467.
[57] M.M. Walker, T.E. Dennis, J.L. Kirschvink, The magnetic sense and its use in long-distance navigation by animals, Curr. Opin. Neurobiol. 12 (2002) 735–744.
[58] J.L. Kirschvink, J.W. Hagadorn, A grand unified theory of biomineralization, in: E. Bäuerlein (Ed.), The Biomineralisation of Nano- and Micro-Structures, Wiley-VCH Verlag GmbH, Weinheim, Germany, 2000, pp. 139–150.